

## **Probing one-dimensional fluctuations in a spin-1/2 antiferromagnetic chain using MACS**

### *1D spin chain:*

Recent developments in neutron instrumentation have allowed the study of fundamentally new phenomena in quantum mechanics. One example, which is the subject of this case study, is the excitation spectrum of the spin-1/2 chain. For a ground state antiferromagnet, the low-energy fluctuations are characterized by propagating spin-waves (or magnons) and these can be derived using first order perturbation theory in a similar way to the calculation of lattice excitations (or phonons). Such theories involve the use of second quantization and starting with an ordered spin ground state and proceeding by calculating transverse spin fluctuations.

While these techniques and theories have been largely successful in describing the low-energy excitations in a variety of materials, they do not take into account quantum effects which become important in investigating the fluctuations of low spin magnets. The quantum corrections owing to the value of the spin, are elegantly expressed by the following Laurent series for the correction to the spin-wave velocity for a two-dimensional Heisenberg antiferromagnet derived by Igarashi [1],

$$Z_p = 1 - \frac{0.1579}{2S} - \frac{0.0215 \pm 0.0002}{(2S)^2} + \dots,$$

where  $Z_p$  is a renormalization factor of the spin-wave velocity. It can be seen from inspection that larger the spin-values ( $S$ ), the less important the corrections. However, for small spin-values and in particular the case of  $S=1/2$ , the corrections become large and therefore a careful treatment of the spin dynamics must take into account quantum mechanics.

The example of a spin-1/2 antiferromagnetic chain is an extreme case as it involves both low spin and also low-dimensionality. The  $S=1/2$  antiferromagnetic one-dimensional nearest neighbor model is described by the Hamiltonian

$$H = J \sum_r \mathbf{S}_r \cdot \mathbf{S}_{r+1}$$

The ground state does not exhibit long-range order, as was first found by Bethe [2], and differs significantly from the Neel type order found in a classical model. Classical antiferromagnetic chain can be readily solved using perturbation theory and the analysis produces the low-energy dispersion to have the following form.

$$E = J|\sin(Q)|$$

This relation has been confirmed in a number of linear-chain antiferromagnets with the classical  $S=5/2$  system (TMMC) being a prototypical example [3].

For  $S=1/2$ , the solution is quite different. Des Cloizeaux and Pearson showed that the lowest-lying excited states are given by the following formula [4]:

$$\text{dcP relation: } E = \frac{\pi}{2}J|\sin(Q)|$$

In this case study, we will evaluate the validity of this expression and characterise the dynamics of a spin-1/2 chain (CuPzN).

### *S=1/2 one-dimensional chain (CuPzN):*

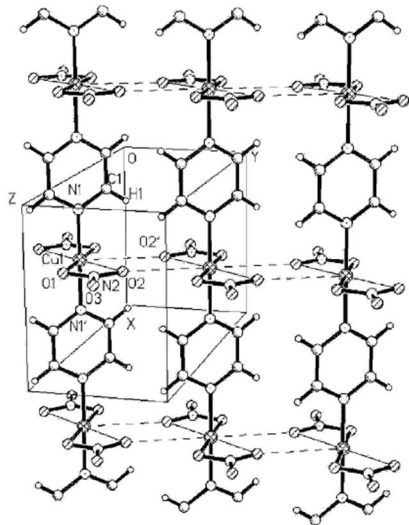


**Figure 1:** Crystal structure of CuPzN showing the  $\text{Cu}^{2+}$  ions (hatched spheres) are linked through pyrazine rings to form one-dimensional chains.

Given that the pyrazine provides the means of the superexchange (and the coupling between  $S=1/2$  Copper ions), the magnetic dynamics are expected to be highly one-dimensional. The chains are held together by strong covalent bonds, where the bonding between chains is due to much weaker Van der Waals forces.

CuPzN,  $(\text{Cu}(\text{C}_4\text{H}_4\text{N}_2)(\text{NO}_3)_2)$  is orthorhombic with space group *Pmna*. The magnetic copper ions form chains along the [100] direction, with one copper unit cell along the chain [5]. The Cu ions along the chain are coupled magnetically through the pyrazine molecules, as illustrated in Fig. 1.

The crystals studied here were grown by slow evaporation of aqueous solutions of Cu(II) nitrate and the corresponding pyrazine. Large single crystals formed after several months with faster evaporation resulting in smaller needle like crystals. The sample used here has total mass of 73 mg and consists of two crystals coaligned with a mosaic (i.e. intrinsic spread of crystal plane

The small mass of the sample (73 mg) is not typical for inelastic neutron scattering experiments. For a conventional cold triple axis instrument, it takes several days of “beam time” to get a full map of the reciprocal space [6]. MACS has the benefit of a high neutron flux and large detector angle coverage, allowing the same range of reciprocal space to be covered in a few hours rather than days.

### *MACS Cold triple-axis spectrometer:*

To investigate the spin fluctuations in this one-dimensional system, the MACS cold triple-axis spectrometer was used. MACS consist of 20 spectroscopic detectors which are used in conjunction with a double bounce graphite analyzer. Further details on MACS will be provided during the presentation and tutorial. For this experiment, a fixed final energy of 5meV was used and the sample was cooled using a helium-4 (ILL orange) cryostat.

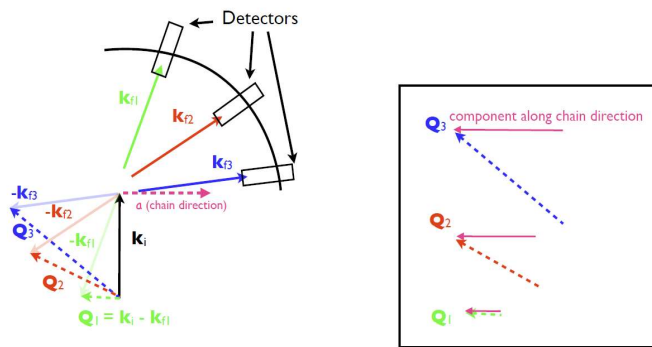


Figure 2. Directions of the incident beam ( $k_i$ ) and scattered beam ( $k_f$ ) with respect to the spin chain.

The sample was aligned in the HK0 scattering plane. The reduced dimensionality means that the excitations will be roughly dispersionless perpendicular to the chain direction and can be summed over without losing information. To map out the excitations, the chain axis was placed perpendicular to the incident beam so that all detectors sampled a unique value along the  $\mathbf{a}$  direction. This is a unique method that can be used in low-dimensional systems and allows the use of multi-detector systems to be of great value in the study of these systems. Further examples of how this has been used effectively for the study of other low-dimensional magnets (such as the cuprate superconductors) will be discussed during the tutorial.

#### *Question:*

*Why the spin chain is aligned perpendicular to the incident beam?*

*Do you expect to get the same information if you align the spin chain parallel to the incident beam? Why?*

## Des Cloizeaux and Pearson (dCP) relation:

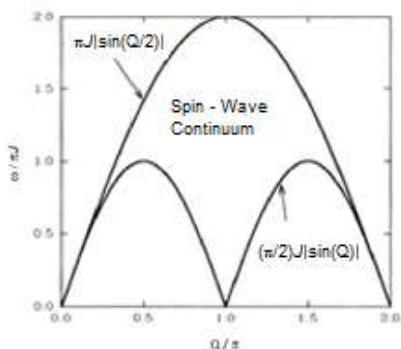


Figure 3: A schematic of the spin-wave dispersion for a linear chain.

During the first part of this tutorial, verify the dCP relation for CuPzN from the data extracted. Perform constant-Q cuts through the data and extract a value for the super exchange constant from the relation provided above.

Take a close look at the lineshapes from a constant-Q scan through the data. Are the peak widths symmetric and resolution limited? Do they represent well defined propagating spin-wave modes?

A careful investigation of the dispersion illustrates that while the overall dispersion seems to follow the dCP relation, there is a distinct high-energy tail to the lineshapes. A constant-Q slice illustrates the presence of a continuum lineshape which as first observed in the one-dimensional chain KCuF<sub>3</sub>. A schematic of the excitation spectrum is presented in Figure 3.

## Spinons:

Verify the dispersion above (and illustrated in Fig. 3) through the use of constant-Q slices. The high-energy continuum represents the fundamental excitation of S=1/2 chain known as a spinon. These excitations can also be interpreted as domain walls or solitons of the ordered antiferromagnetic background. [7]

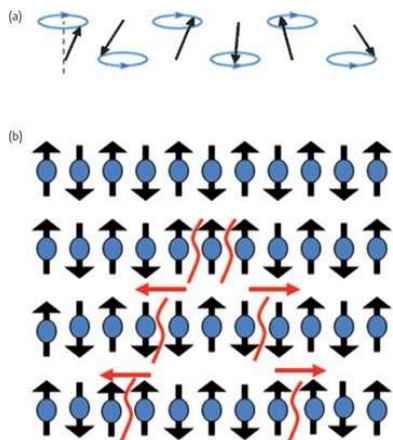


Figure 4: Description of spinons and compared to linear transverse spin-wave excitations.

The experimental signature of this excitation is significant spectral weight observed over a broad range in momentum and energy transfer. Because the excitations are broad in energy and momentum, they are typically quite difficult to measure and characterize and were first measured in the linear chain KCuF<sub>3</sub> using the MARI chopper time-of-flight spectrometer at ISIS [8]. The presence of a multi detector array and large incident flux, such as available on MACS, allows these types of excitations to be readily measured and characterized.

*Questions:*

*Why do spinons produce a continuum in neutron scattering?*

## *The Multi-Axis Crystal Spectrometer (MACS)*

The MACS instrument is located at BT 9 with its own cold source to optimize neutron flux to the sample. The high neutron flux reaches up to  $3 \times 10^8$  neutrons/cm<sup>2</sup>/s. The front-end includes radial collimators and beam apertures to optimize Q-resolution, energy resolution and flux on the sample. The high neutron flux is obtained by using a 1428 cm<sup>2</sup> doubly focusing monochromator subtending a solid angle of up to 0.005 Sr to the NIST cold neutron source (Figure 5). The spectrometer is designed for wave vector resolved spectroscopy up to 20.0 meV transfer with a resolution down to 0.05 meV. The back end of the spectrometer includes a detector system with an array of 20 channels which combined subtend a solid angle of 0.2 Sr to the sample. Each detector channel is built around a vertically focusing double crystal analyzer for enhanced signal to noise. The MACS instrument is particularly powerful for probing the wave vector dependence of inelastic neutron scattering in select ranges of energy transfer to access the dynamic structure of fluctuating systems [9].

The neutronic input is a diverging filtered cold neutron beam with a circular cross section. The rotating beam shutter has three aperture options and is placed on the experimental floor immediately outside the biological shielding. This enables extraction of the full beam cross section from the source. The cryo-filter exchanger is located downstream of the shutter; this system allows cooled beryllium, graphite and, in the future MgF<sub>2</sub>, filters to be positioned between the beam shutter and the monochromating system. Two radial collimators A and B which limit horizontal beam divergence incident on any volume element of the monochromator, can be placed after the filter. This provides four different collimation settings: open A, B and A+B which limits the horizontal divergence of radiation incident on a volume element of the monochromator to 60', 40' and 24', respectively. Radially focused to the source, these collimators effectively function as source apertures to control the incident beam energy resolution.

A vertical and horizontal beam aperture can be varied automatically from closed to a 35 cm by 35 cm square. By defining the overall envelope of the beam in the horizontal and vertical planes, this aperture determines the transverse to  $k_i$  wave vector resolution. The doubly focusing monochromator (DFM) was designed to minimize structural materials in the neutron beam in order to reduce background. The DFM consists of an array of 357 pyrolytic graphite (PG) crystals attached to thin aluminum blades that can be bent and rotated to control vertical and horizontal focusing, respectively (Figure 6). To increase the range of incident energies while

limiting the motion of the large detector system, the monochromator is moved along the reactor beamline to access different energies.

The monochromatic beam reaches the sample via a converging channel and beamline shielding system, named, the monochromatic beam transport system (MBT). The beam channel is lined by a super-mirror guide and the horizontal dimension is variable so the beam profile can be optimized. This trumpet shaped guide should increase the flux, by further broadening the transverse wave vector resolution. Immediately before the sample position there are vertical and horizontal beam slits to further crop the beam so only the sample is illuminated. There is also single crystalline LiF attenuators with absorption factors of 1/10 and 1/100 respectively, which can be introduced into the beam under computer control. The sample table contains no magnetizable materials within 75 cm of the sample position and can support sample environment systems weighing up to 400 kg.

The detection system (Figure 7) consists of 20 identical channels surrounding the sample and separated by 8 in the horizontal scattering plane. Each channel is defined by a cast structure formed from neutron absorbing  $B_4C$  in polyurethane. Each channel contains a 90° soller collimator. Each channel includes three different filters (Be, BeO and graphite) cooled to less than 77 K to reduce transmission losses from inelastic scattering. Each channel also contains a vertically focusing double crystal analyzer (DXAL). Each of the two analyzer blades consists of nine PG (0 0 2) crystals with dimensions 6.0 cm wide, 2.0 cm tall and 0.2 cm thick, mounted to form the surface of a cylinder with radius 50 cm. These can be rotated about the center of mass of the reflecting graphite. Based on a system developed for use as an x-ray monochromator, the DXAL mechanism both rotates and translates the two analyzer blades to transmit energies between 2.5 meV and 20 meV. This motion is actuated by a single stepping motor per DXAL and all alignment is achieved mechanically. The distance from the sample to the DXAL rotation axis is 100.0 cm and the perpendicular distance between the two analyzer translation stages within one DXAL is 7.00 cm. There are two detectors in each of the 20 channels. The so-called diffraction detector that views the sample directly is placed behind the first analyzer. The spectroscopic detector views the second analyzer blade and so only detects neutrons that satisfy the DXAL Bragg condition. It is possible to set different final energies for each analyzer, take Q area scans for a common final energy or operate the instrument as a virtual triple axis spectrometer focusing on the signal in a single channel of interest, employing always the most convenient channel for the desired scattering angle.

*Questions:*

*We have determined from previous zero-field susceptibility measurements that  $J=0.91$  meV. What energy range are we interested on?*

*What  $E_f$  and  $E_i$  should I choose? Why?*

*Should I use a Neutron filter for the incident and scattered beam? If so, which filter(s)? Why?*

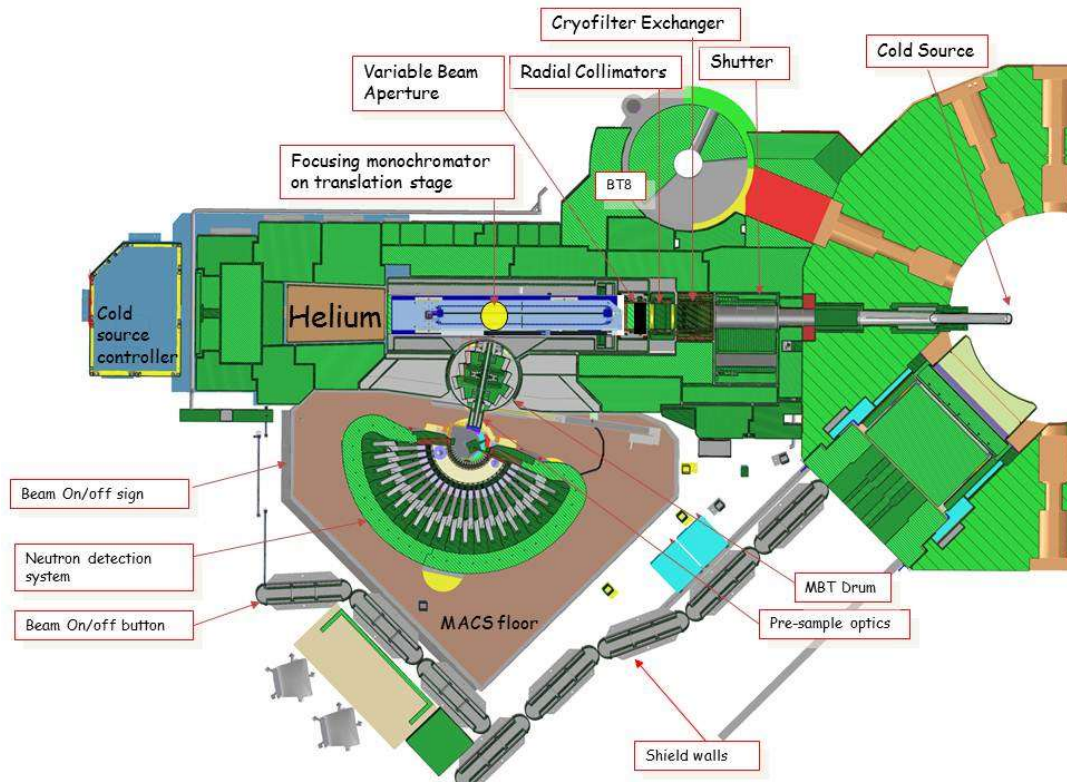


Figure 5: Schematic top view of MACS

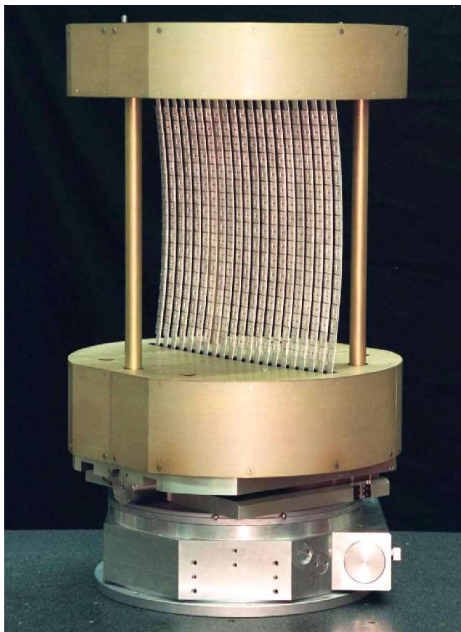


Figure 6: Doubly Focusing Monochromator (DFM). The DFM consist of 21 blades with 17 HOPG 2 cm x 2 cm crystals per blade. The blades can be bended and rotated to control the vertical and horizontal focus.

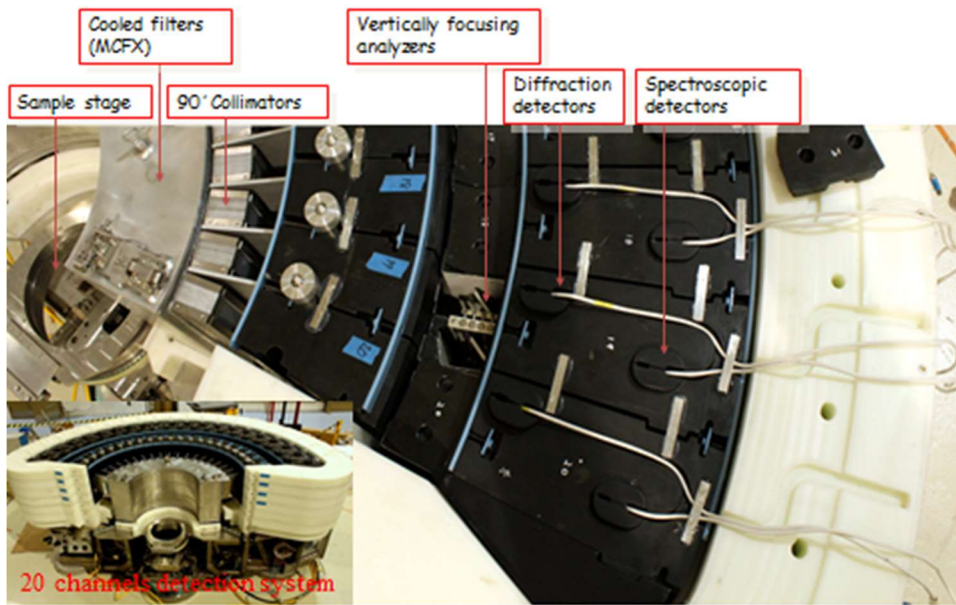


Figure 7: MACS detector system

## References:

- [1] Igarashi, Phys. Rev. B **46**, 10763 (1992).
- [2] H.A. Bethe, Z. Phys. **71**, 205 (1931).
- [3] M.T. Hutchings et al, Phys. Rev. B **5**, 1999 (1972).
- [4] J. Des Cloizeaux and J.J. Pearson, Phys. Rev. **128**, 2131 (1962).
- [5] P.R. Hammar et al., Phys. Rev. B **59**, 1008 (1999).
- [6] M. B. Stone et al. Phys. Rev. Lett. **91** 037205 (2003)
- [7] B. Lake, Nature Physics **1**, 143 (2005)
- [8] S.E. Nagler et al., Phys. Rev. B **44**, 12361 (1991).
- [9] J. A. Rodriguez et al. Meas. Sci. Technol. **19** 034023 (2008)